The Meteoritical Society

Meteoritics & Planetary Science 1–17 (2019)
doi: 10.1111/maps.13374

Northwest Africa 10414, a pigeonite cumulate shergottite

R.H. HEWINS[1,2*], B. ZANDA[1,3], S. PONT[1], and P.-M. ZANETTA[4]

[1]Institut de Minéralogie, de Physique des Matériaux, et de Cosmochimie (IMPMC), Sorbonne Université, Muséum National d'Histoire Naturelle, UPMC Université Paris 06, UMR CNRS 7590, IRD UMR 206, 61 rue Buffon, 75005 Paris, France
[2]Earth and Planetary Sciences, Rutgers University, Piscataway, NJ 08854, USA
[3]IMCCE, Observatoire de Paris, CNRS UMR 8028, 77 Av. Denfert Rochereau, 75014 Paris, France
[4]Université Lille, CNRS, UMR 8207, UMET, 59000 Lille, France
[*]Corresponding author. E-mail: hewins@scarletmail.rutgers.edu

(Received 07 February 2018; revision accepted 22 July 2019)

Abstract–Northwest Africa (NWA) 10414 is an unusual shergottite with a cumulate texture. It contains 73% coarse prismatic pigeonite, plus 18% interstitial maskelynite, 2% Si-rich mesostasis, 2% merrillite, and minor chromite-ulvöspinel. It contains no olivine, and only ~3% augite. Phase compositions are pigeonite ($En_{68-43}Fs_{27-48}Wo_{5-15}$) and maskelynite $An_{\sim 54-36}$, more sodic than most maskelynite in shergottites. Chromite-ulvöspinel composition plots between the earliest and most fractionated spinel-group minerals in olivine-phyric shergottites. NWA 10414 mineralogically resembles the contact facies between Elephant Moraine 79001 lithologic units A and B, with abundant pigeonite phenocrysts, though it is coarser grained. Its most Mg-rich pigeonite also has a similar composition to the earliest crystallized pyroxenes in several other shergottites, including Shergotty. The Shergotty intercumulus liquid composition crystallizes pigeonite with a similar composition range to NWA 10414 pigeonite, using PETROLOG. Olivine-phyric shergottite NWA 6234, with a pure magma composition, produces an even better match to this pigeonite composition range, after olivine crystallization. These observations suggest that after the accumulation of olivine from an olivine-phyric shergottite magma, the daughter liquid could precipitate pigeonite locally to form this pigeonite cumulate, before the crystallization of overlying liquid as a normal basaltic shergottite.

INTRODUCTION

The SNC meteorites (shergottites, nakhlites, and chassignites) have long been recognized as planetary igneous rocks (Papanastassiou and Wasserburg 1974; Reid and Bunch 1975) from Mars (Bogard and Johnson 1983). The shergottites, the most abundant Martian meteorite type, are a chemically and mineralogically diverse set of basaltic rocks. They reflect significant variation in mantle source regions, magma transport mechanisms, and conditions of crystallization. While shergottites are critical to understanding Mars' evolution, they are complex. They are divided into three main categories—poikilitic, olivine-phyric, and basaltic (Goodrich 2002; Bridges and Warren 2006; Shearer et al. 2008; Papike et al. 2009; Walton et al. 2012), with three superimposed chemical types—enriched, intermediate, and depleted in incompatible trace elements. There are several mineralogical or textural variants, for example, Northwest Africa (NWA) 6963 (Filiberto et al. 2018), NWA 7635 (Lapen et al. 2017), and NWA 8159 (Herd et al. 2017). A significant development is the recognition of Al-rich and Al-poor shergottite suites, each modified by fractional crystallization, and each having the wide range of incompatible element concentrations (Treiman and Filiberto 2015), that clarify the roles of mixing and fractionation of these magmas.

Stolper and McSween (1979) and McSween et al. (1979a, 1979b) proposed that olivine-saturated magmas were parental to the basaltic shergottite suite. Experimental studies of the basaltic shergottites Shergotty and Zagami were expected to produce coexisting pigeonite and augite at liquidus temperatures (McKay et al. 2000), but only pigeonite was observed as

their liquidus phase (Stolper and McSween 1979; McCoy and Lofgren 1999; McKay et al. 2000; Dann et al. 2001). Elephant Moraine (EET)-A 79001 is a key sample with an igneous contact between olivine-phyric facies A and basaltic shergottite facies B (McSween and Jarosewich 1983; Goodrich 2003; Van Niekerk et al. 2007), with a pigeonite-rich contact zone. Goodrich (2003) argued that EET-B was the fractionated liquid lost after olivine phenocrysts were accumulated in EET-A, and other olivine-phyric parent and basaltic daughter pairs have been proposed (Filiberto et al. 2012; Treiman and Filiberto 2015). In EET-B, pigeonite crystallized before augite, as in many shergottites, providing the possibility of making a pigeonite cumulate after olivine has settled. The ~1 cm wide pigeonite-rich contact facies of EET-B with EET-A may thus have formed by settling of pigeonite (Van Niekerk et al. 2007).

Northwest Africa 10414 is an unusual shergottite relevant to the relationship between olivine-phyric and basaltic shergottites. It contains pigeonite but not olivine and very little augite. The study of NWA 10414 clarifies the conditions of pigeonite crystallization and its role in the transition from olivine-phyric to basaltic shergottites.

SAMPLE AND METHODS

An 8 g sample of NWA 10414 was cut at the Institut de Minéralogie, de Physique des Matériaux, et de Cosmochimie (IMPMC), Muséum National d'Histoire Naturelle (MNHN), to prepare a polished section numbered AK for study using reflected light microscopy, scanning electron microscopy (SEM), Raman microspectroscropy, and electron probe micro analysis (EPMA). A backscattered electron (BSE) map and images of selected regions were made at MNHN using a Tescan VEGA II LSU SEM in conventional mode (mainly 15 keV, <20 nA, and 15.4 mm working distance). High resolution images were made at the IMPMC quarters at the Université Paris VI, using a Zeiss Ultra 55 field emission (FE) SEM using 15 keV and 7.5 mm working distance.

Modal analysis was achieved using a simplified version of the ACADEMY method (Zanetta et al. 2019). We acquired Si, Fe, Mg, Ca X-ray maps of the entire section on the VEGA SEM with 4 μm pixels and prepared a phase map. Using Matlab®, we selected the pixels of similar composition to reveal the localization of the different grains. Reference grains were later used to classify all pixels by K-means clustering, using XMapTools (Lanari et al. 2014). The large map allowed us to select a smaller representative area, for analysis at greater resolution and with a greater number of counts/pixel. We then acquired a hyperspectral map that was processed using Hyperspy (de la Peña et al. 2017). This map was acquired on a representative 3.62 mm² region with a resolution of 2048 × 2048 pixels (1.7 μm/pixel). Compositional endmembers for eight phases were extracted. To construct the phase map and obtain a higher number of counts, the signal was rebinned to a 250 × 250 pixel hyperspectral map (10 μm/pixel) which was still sufficient to resolve most of the smaller grains. A convolution of these different reference spectra was fitted to the raw data. This allowed us to construct a more precise phase map and to estimate mixing proportions in pixels using the scaling coefficient of the model components (Zanetta et al. 2019).

Minerals were characterized on the MNHN SEM with an SD^3 (Bruker) EDS detector. We used an inVia confocal Raman microscope with a 532 and 785 nm laser sources at MNHN for distinguishing feldspar phases and silica phases. All quantitative mineral analyses were made by wavelength-dispersive spectrometry on the Cameca SXFive electron microprobe at the Université Paris VI equipped with an LaB_6 source, mainly using 15 keV and 10 nA, but 10 kev and 20 nA for some phosphates, with a focused beam or small rasters. Dwell time was 10 s for peaks and backgrounds, increased to 20 or 60 s for some minor elements, for example, Mn. We used silicate, oxide, and phosphate standards, and checked the calibrations with San Carlos and Eagle Station internal standards.

PETROGRAPHY

Northwest Africa 10414 consists mainly of an aggregate of euhedral, highly fractured, weakly zoned pigeonite prisms, up to 4 × 1 mm in size, with a cumulate texture (Figs. 1a and b). The pigeonite prisms are set in interstitial maskelynite-rich mesostasis patches. Augite is seen in X-ray map (Fig. 2) as interstitial grains, small grains in mesostasis, and as inclusions in pigeonite. Si-rich inclusions and maskelynite inclusions are also seen within pigeonite. Some apparent inclusions of augite are shown to be interstitial between two crystals of pigeonite by differences in orientation of exsolution lamellae (Fig. 3a). Maskelynite laths have euhedral Ca-rich cores visible in enhanced BSE (Fig. 1b), and zonation, though in normal contrast the feldspar appears to be smooth unfractured maskelynite. Raman spectra show weak broad peaks near 500 and 600 cm^{-1} characteristic of maskelynite (Fritz et al. 2005). The preservation of zoning suggests solid-state formation though the maskelynite flowed elsewhere, in shock melt pockets.

A low-resolution phase map generated from X-ray images of the section is shown in Fig. S1 in supporting information. A higher resolution phase map (with binned 1.7 μm pixels) of a representative 3.62 mm region was prepared (Fig. S2 in supporting information),

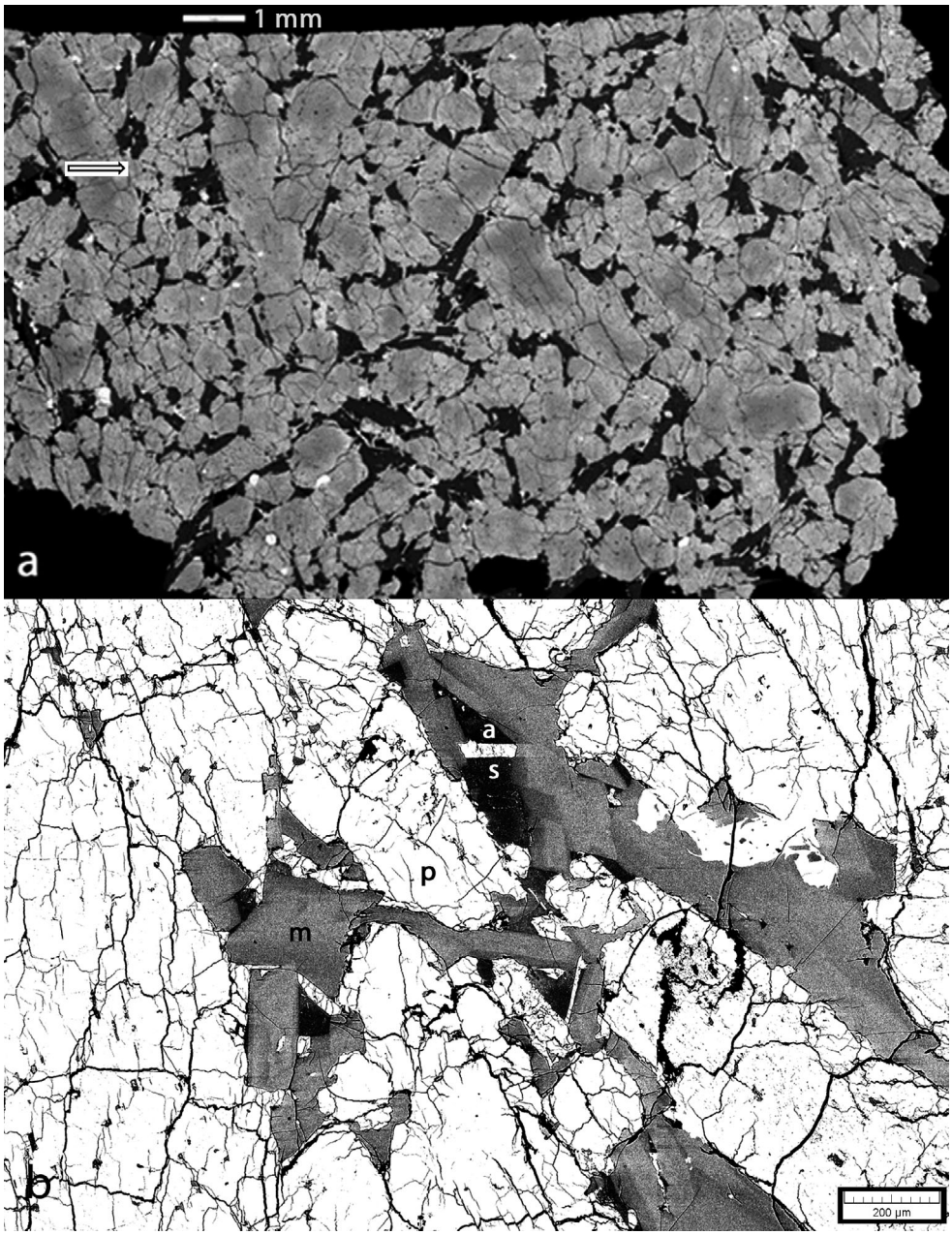

Fig. 1. Backscattered electron (BSE) images of a polished section of Northwest Africa 10414 (BSE) showing cumulate texture. a) Pigeonite (gray with light gray rims), chromite (white), merrillite needles (off-white), and interstitial maskelynite and mesostasis (both dark gray). b) Cumulus pigeonite (p, white), with interstitial maskelynite laths (m, medium gray) and Si-rich residual melt (s, dark gray) containing merrillite needles (a, white). The arrow shows the position of the pyroxene traverse of Fig. 5c.

using the ACADEMY approach of Zanetta et al. (2019), and phase abundances were calculated, as shown in Table 1.

Of the minor phases, chromite-ulvöspinel occurs mainly as inclusions in pigeonite, and merrillite (~1%) mainly as blades in mesostasis, though it is also found within pigeonite. Apatite occurs as thin rims on some merrillite blades. Other accessory minerals include a silica phase, alkali feldspar, ilmenite, baddeleyite, and pyrrhotite. The pigeonite contains small blocky or irregular Si-rich inclusions typically < 100 µm in size (Fig. 3b), both sodic and potassic, as well as ~100 nm exsolution lamellae. Based on the good stoichiometry of the pigeonite analyses, these lamellae must be augite. The mesostasis consists primarily of an intergrowth of 1–10 µm sodic plagioclase closely intergrown with a

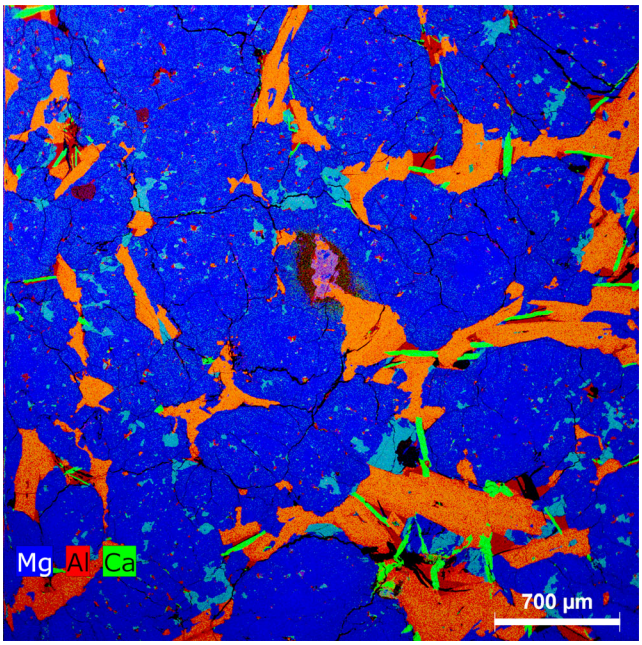

Fig. 2. Combined elemental map for Mg (blue), Al (red), and Ca (blue) K X-rays, showing pigeonite (dark blue), maskelynite (orange), augite (light blue), merrillite (brown), Si-rich mesostasis (brown).

silica phase, similar to that in NWA6963 (Filiberto et al. 2014) but finer grained (Fig. 3c). Ilmenite as well as baddeleyite have been identified in mesostasis, though they are more prominent in association with small SiO_2-rich inclusions within pigeonite margins against mesostasis (Fig. 3d). The rock is unaltered except for miniscule barite granules peppering one or two pigeonite grains, and isolated Fe-rich phases associated with local high Mn and Ba concentrations in shocked pigeonite, probably related to desert weathering.

The meteorite is moderately shocked, containing a few small (~200 μm) patches of shock melt at some pigeonite-maskelynite contacts (Fig. 4a). The melt is Si-rich and both P- and S-bearing, due to melting of pyroxene and feldspar, and accessory phases. It contains smooth anhedral grains of pyroxene and silica up to ~30 μm in size, as well as merrillite. Its groundmass is heterogeneous on a submicron scale (Fig. 4b), containing Fe-rich phase(s), and its texture resembles that of shock veins in Zagami (El Goresy et al. 2013). The silica grains are surrounded by micron-thick rims of denser glass. The pyroxene and merrillite may be unmelted relicts, but silica grains of this size are rare in the unshocked regions suggesting that they were produced by the shock. Both high pressure polymorphs of silica and silica glass (lechatelierite) occur in shergottites (El Goresy et al. 2013). The silica in NWA 140414 lacks fractures and has Raman spectra without characteristic peaks suggesting that it is glass. Stoichiometric maskelynite occurs as veins in the impact melt, which in turn is interfingered into the melt (Fig. 4a). Any mixing between the two is at a submicron level. Pigeonite adjacent to the shock melt contains lamellar to fibrous deformation features, with lamella orientation changing on a scale of 10–20 μm (Fig. 4c). This pigeonite contains pyrrhotite inclusions, and streaks of Mg-free silicate and Fe oxide or hydroxide parallel to exsolution lamellae ~100 nm in width (Fig. 4d).

MINERAL COMPOSITIONS

Northwest Africa 10414 pyroxene has an Fe/Mn atomic ratio of 34.2 SD 3.0 (n = 75) compared with an average value of 32 SD 6 for Martian basalts (Papike et al. 2003). The data plot on or slightly below the best fit line on the Fe-Mn plot of Papike et al. (2009) for pyroxene-phyric basalts, confirming the Martian origin of NWA 10414. The pigeonite crystals are normally zoned with Ca, Fe, Mn, and Ti increasing, and with Mg and Cr decreasing toward the rims. Pigeonite core and rim composition ranges from $En_{68}Fs_{27}Wo_5$ to $En_{43}Fs_{48}Wo_{15}$, and for interstitial augite, it is $En_{43}Fs_{28}$ Wo_{37} to $En_{38}Fs_{28}Wo_{34}$ (Fig. 5a; Table 2). The composition range across a single ~1 mm wide pigeonite prism is ($En_{65}Fs_{29}Wo_6$ to $En_{48}Fs_{41}Wo_{11}$) (Figs. 5b and 5c; Table 2) matching the middle of the range for random grains given above traverse across this pigeonite prism revealed a ~15 μm inclusion of orthopyroxene in the interior and one of augite near the rim, neither of which could be distinguished in BSE. These compositions are indicated in the quadrilateral Fig. 5b and the traverse Fig. 5c.

The plagioclase (maskelynite) composition is $An_{46.7 \pm 3.9}Ab_{50.8 \pm 3.4}Or_{2.5 \pm 0.6}$ (n = 111), with a range of $An_{\sim 54-38}$ (Fig. 6a; Table 2). Individual maskelynite pseudomorphs after plagioclase laths are slightly zoned and differ from one another (Fig. 6b). Most shergottites contain more calcic early formed plagioclase than this (Basu Sarbadhikari et al. 2009). This is shown in Fig. 6a, for Shergotty and Zagami (Stolper and McSween 1979), EET 79001A, EET 79001B, and QUE 94201 (Mikouchi et al. 1998, 1999), NWA 1068 (Barrat et al. 2002b), NWA 2990 (Bunch et al. 2009), NWA 5718 (Wittke et al. 2010), NWA 5789 (Gross et al. 2011), NWA 6234 (Gross et al. 2013), and Los Angeles (Warren et al. 2004). The exceptions with less calcic early formed plagioclase are the enriched olivine-phyric shergottites NWA 1068 (Barrat et al. 2002b) and LAR 06319 (Basu Sarbadhikari et al. 2009). NWA 6963 is similar, though it contains rare calcic grains (Filiberto et al. 2014).

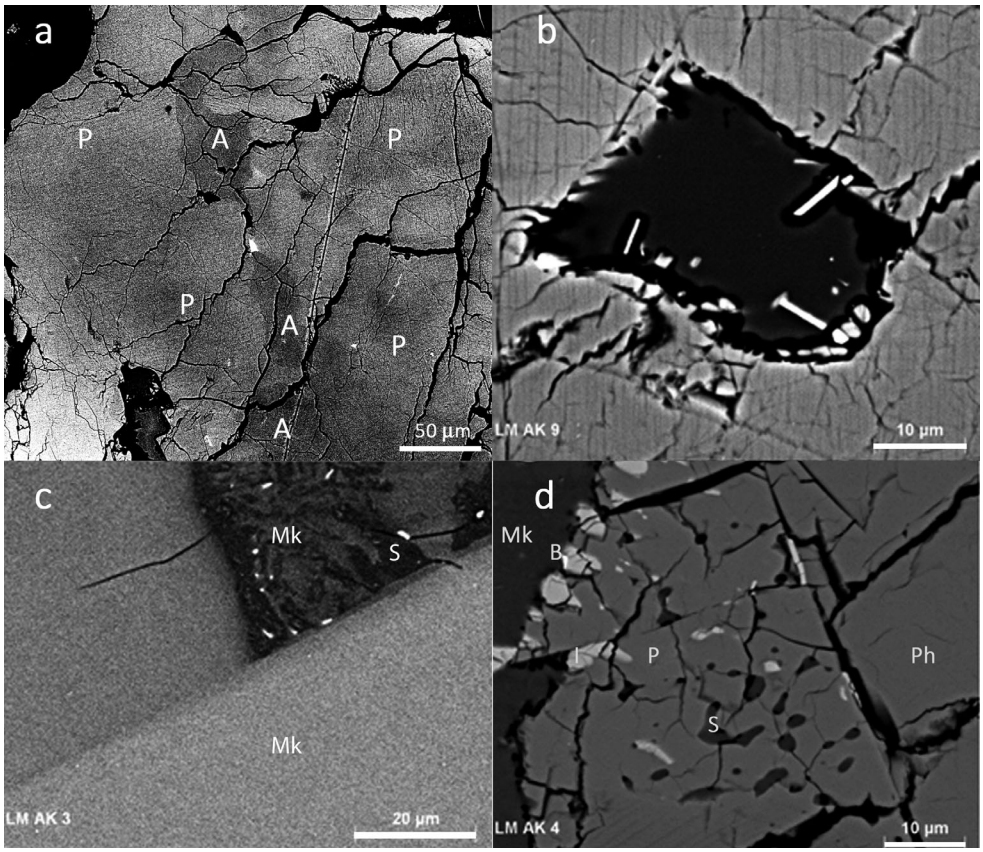

Fig. 3. Backscattered electron images of Northwest Africa 10414. a) Interstitial augite grains between two crystals of pigeonite. b) Na-KSi-rich inclusion containing three ilmenite needles and phosphate specks, in pigeonite with ~200 nm augite lamellae. c) Interstitial mesostasis with an intergrowth of sodic maskelynite and a silica phase, plus baddeleyite and ilmenite specks. d) Pigeonite (with fine SiO_2 inclusions, and ilmenite with baddeleyite), mesostasis (left), and merrillite (right). A is augite, B baddeleyite, I ilmenite, Mk maskelynite in mesostasis, P pigeonite, Ph merrillite, S silica.

Table 1. Modal abundances.

Pigeonite	72.58%
Maskelynite	17.93%
Augite	3.41%
Chromite-ülvospinel	0.39%
Merrillite	2.03%
Pyrrhotite	0.21%
Si-rich mesostasis	1.92%
Shock melt	1.54%
Total	100.00%

Chromite-ulvöspinel compositions in NWA 10414 range from ~$Spl_{21}Chr_{65}Usp_6Mag_8$ to ~$Spl_4Chr_1Usp_{49}Mag_{46}$ (Table 2). They are compared in Fig. 7 to those for Tissint and 10 other olivine-phyric shergottites (Allan Hills (ALH) 77005, Dar el Gani (Dag) 476, Dhofar (Dho) 019, Elephant Moraine (EET) 79001A, Larkman Nunatak (LAR) 06319, NWA 1068, NWA 1110, NWA 5789, NWA 6234, and Sayh al Uhaymir (SaU) 005). Olivine-phyric shergottite data shown are from Mikouchi et al. (2001), Barrat et al. (2002b), Goodrich et al. (2003), Basu Sarbadhikari et al. (2009), and Gross et al. (2011, 2013) and we show separately our own data for Tissint (Chennaoui Aoudjehane et al. 2012). NWA 10414 oxide minerals are not quite as Cr-rich as chromites crystallized along with olivine in other shergottites (e.g., Goodrich et al. 2003) and are continuously fractionated to almost Cr-free compositions. Their Fe and Ti fractionation trend involves strong enrichment in Fe^{3+}, as for most olivine shergottites but is unlike the trend more toward the ulvöspinel endmember for Tissint, Dar al Gani 476 (Mikouchi et al. 2001), and NWA 5789 (Gross et al. 2011). In basaltic shergottites, the spinel phase is mainly Cr-poor titanomagnetite (Stolper and McSween 1979; Goodrich et al. 2003) except in those with liquidus magnesian pyroxene like NWA 480 (Barrat et al. 2002a).

The ilmenite is near-endmember $Ilm_{99\text{-}94}Hem_{01\text{-}06}$. Since ilmenite coexisting with magnetite normally increases its Ti content with decreasing temperature

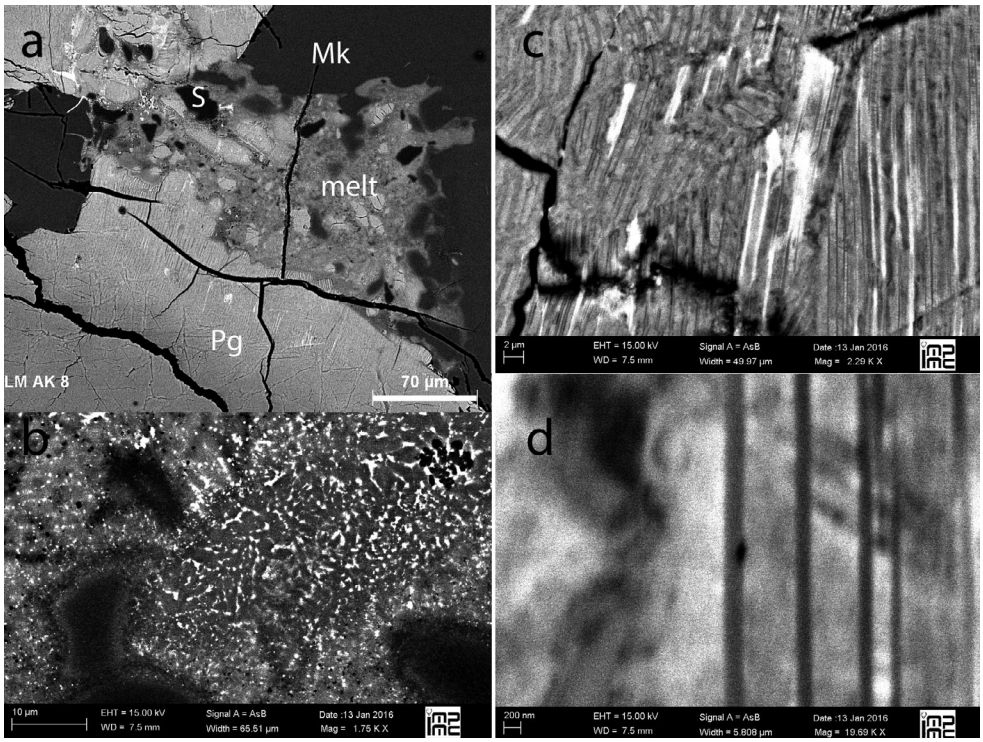

Fig. 4. Backscattered electron images. a) Patch of heterogeneous shock melt (melt) between pigeonite grains and maskelynite, with silica inclusions (black) and interfingering or veining of the P- and S-bearing silicate melt with mobilized maskelynite. b) Groundmass of shock melt pocket. c) Pigeonite adjacent to shock melt is lamellar to fibrous and deformed, with pyrrhotite inclusions, streaks of Mg-free silicate, and Fe oxide or hydroxide. d) Pigeonite contains exsolution lamellae ~100 nm in width. Symbols as before.

(e.g., Buddington and Lindsley 1964), we assumed the most Ti-poor ilmenite coexisted in the groundmass with the most ferrian titanomagnetite ~$Spl_4Chr_1Usp_{49}Mag_{46}$. Such an assemblage would indicate equilibration at 825 °C and an oxygen fugacity (fO_2) of FMQ–0.3 log units, with standard deviations of 6 °C and 0.2 log units based on the composition range observed, calculated using the method of Sauerzapf et al. (2008). This temperature is consistent with oxide assemblages that equilibrated at ~800 °C in many shergottites (Herd et al. 2001). The calculated fO_2 is high for shergottites but similar to values for Shergotty (Herd et al. 2001), NWA 5298 (Hui et al. 2011), and a late stage assemblage in NWA 1110 (Herd 2003). Crystallization modeling (below) suggests that the pigeonite crystallized at a lower fO_2.

Among accessory phases, pyrrhotite in NWA 10414 occurs as small anhedral grains in mesostasis. Its composition is $Fe_{\sim 0.96}S_1$. Apatite rims on merrillite, calculated on a 3 P atomic basis, contain on average 0.40% F, 0.25% Cl, leaving an assumed 0.35% OH.

The mesostasis is seen in the SEM to be a micrographic intergrowth (Fig. 5b) like that in NWA 6963 (Filiberto et al. 2014) though the electron probe excitation volume causes a bulk composition resembling Si-rich glass. In rare cases, the analysis resolved the silica phase, but generally the results are interpreted as mixtures of silica and 40–80% feldspar. The Si and Al contents for bulk mesostasis define mixing lines, which we extrapolate to pure silica plus extremes of plagioclase $Ab_{\sim 68}$ and alkali feldspar $Or_{\sim 66}$ but also to intermediate feldspar.

DISCUSSION

Crystallization of NWA 10414 Compared to That of Other Shergottites

Understanding relationships between shergottites, and particularly olivine-phyric and pyroxene-rich shergottites, requires a knowledge of liquid compositions. Shergotty and Zagami were recognized as phenocryst-enriched basaltic rocks rather than as crystallized parent liquids (McSween et al. 1979a; Stolper and McSween 1979; Hale et al. 1999), but NWA 480 (Barrat et al. 2002a) and QUE 94201 may have the compositions of the liquids from which they crystallized (McSween et al. 1996; Mikouchi et al. 1998; Barrat et al. 2002a; Filiberto and Dasgupta 2011; Gross

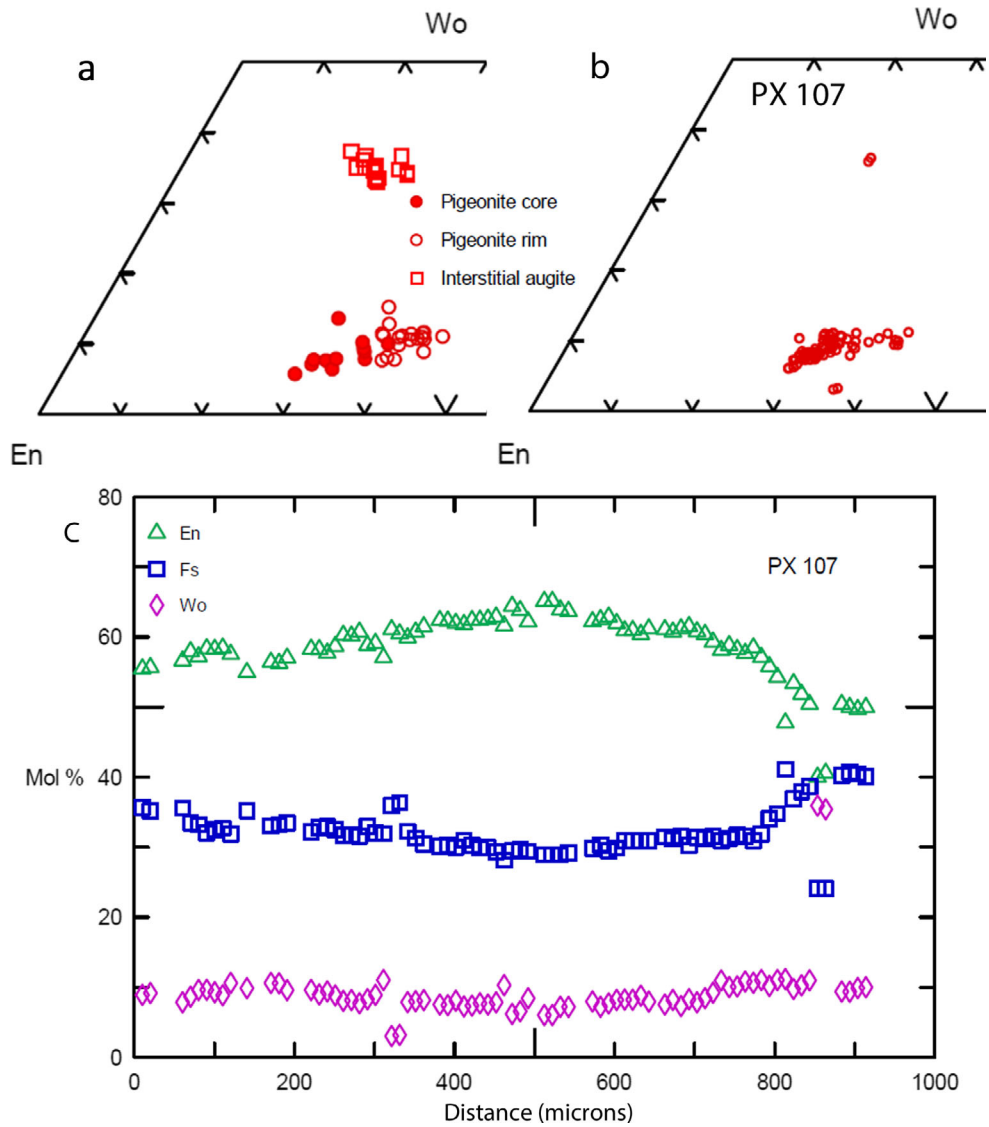

Fig. 5. Pigeonite compositions in Northwest Africa 10414. a) Pyroxene quadrilateral for pigeonite random cores and rims, and augite. b) Analyses of crystal 107; the outlier points are within the crystal. c) Traverse across pyroxene crystal 107 to show zoning; it includes a few points of augite and orthopyroxene.

et al. 2013). In the case of olivine-phyric shergottites, Fe-Mg partitioning between olivine and melt has been used to tell whether olivine was in equilibrium with a liquid of bulk meteorite composition (e.g., Filiberto and Dasgupta 2011). Yamato 980459 (Greshake et al. 2004; Mikouchi et al. 2004; Musselwhite et al. 2006), NWA 5789 (Gross et al. 2011), NWA 2990 (Bunch et al. 2009; Filiberto and Dasgupta 2011), and NWA 6234 (Gross et al. 2013) have bulk compositions that could represent liquid compositions, and many other shergottites have accumulated excess olivine and/or pyroxene.

The silicate crystallization sequences in shergottites have olivine, if present, generally followed by sequential or simultaneous crystallization of two or three pyroxene phases, and then plagioclase (Stolper and McSween 1979; Papike et al. 2009). There is evidence of a Ca-poor pyroxene phase preceding augite, and in part following it (Stolper and McSween 1979; Mikouchi et al. 1999; Van Niekerk et al. 2007; Papike et al. 2009; Herd et al. 2017).

Northwest Africa 10414 differs from other basaltic shergottites in that it has only one major pyroxene, pigeonite. It is a plagioclase-rich pyroxenite or pigeonite orthocumulate with only ~5% augite and no olivine. It has the classic orthocumulate texture as defined by Wager et al. (1960), with limited adcumulus growth on the subhedral pigeonite crystals. It consists mainly of an aggregate of euhedral, highly fractured, weakly zoned

Table 2. Electron microprobe analyses of pyroxene, spinel, and maskelynite in NWA 10414.

Pyroxene	SiO_2	Al_2O_3	TiO_2	Cr_2O_3	FeO	MnO	MgO	CaO	Na_2O	Total	En	Fs	Wo
Pigeonite 61	53.98	0.76	0.12	0.38	17.07	0.60	24.10	2.38	0.04	99.50	68.10	27.06	4.83
Pigeonite 81	53.34	0.84	0.14	0.26	18.55	0.61	21.65	3.70	0.10	99.24	62.37	29.98	7.65
Pigeonite 1	52.78	1.03	0.10	0.22	19.90	0.59	20.79	4.14	0.05	99.68	59.52	31.95	8.53
Pigeonite 39	52.84	0.91	0.33	0.19	22.29	0.68	17.82	5.41	0.11	100.61	52.09	36.54	11.37
Pigeonite 22	51.17	0.73	0.46	0.00	24.86	0.69	15.71	5.38	0.06	99.12	46.85	41.61	11.54
107 C 53[a]	53.55	0.97	0.02	0.32	18.28	0.51	23.06	2.96	0.07	99.77	65.08	28.92	6.00
107 M 36	53.32	0.86	0.17	0.29	19.55	0.62	21.28	3.88	0.07	100.08	60.72	31.29	7.99
107 M 8	52.96	0.90	0.17	0.32	20.92	0.61	20.30	4.20	0.08	100.44	57.91	33.47	8.62
107 R 82	50.76	1.39	0.23	0.38	24.40	0.57	15.88	5.17	0.09	98.94	47.74	41.12	11.14
Augite 23	51.32	2.13	0.38	0.64	13.47	0.40	14.25	16.36	0.20	99.46	42.46	22.52	35.03
Augite 24	51.21	2.30	0.50	0.67	13.16	0.39	14.21	17.03	0.20	99.89	42.01	21.82	36.17
Augite 3	50.98	1.55	0.43	0.58	14.50	0.40	14.16	16.30	0.22	99.51	41.64	23.92	34.44
Augite 4	51.49	1.09	0.96	0.21	16.38	0.46	13.13	16.54	0.20	100.88	38.39	26.86	34.75
Augite 25	51.42	0.98	0.79	0.20	17.09	0.59	12.80	15.98	0.23	100.27	37.80	28.30	33.90

Spinel	SiO_2	Al_2O_3	TiO_2	Cr_2O_3	FeO	MgO	Total	Spl	Chr	Usp	Mag
62/1	0.13	10.04	2.09	46.34	33.97	4.07	96.67	20.99	65.02	5.61	8.37
67/1	0.11	5.39	6.30	38.75	44.19	2.30	97.05	11.60	55.96	17.29	15.15
17		3.13	15.60	21.58	55.44	1.50	97.25	6.86	31.65	43.54	17.95
16		3.38	17.31	16.12	58.96	1.52	97.30	7.36	23.56	48.14	20.94

Maskelynite	SiO_2	Al_2O_3	TiO_2	Cr_2O_3	FeO	MgO	CaO	Na_2O	K2O	Total	An	Ab	Or
20	54.29	28.04	0.04		0.75	0.08	11.10	5.12	0.30	99.85	53.56	44.75	1.70
33	55.50	27.73	0.07		0.50	0.06	10.09	5.64	0.33	99.91	48.78	49.34	1.88
14	56.01	27.04	0.08		0.58	0.03	9.70	5.80	0.48	99.76	46.71	50.55	2.74
10	56.99	26.34	0.14		0.73	0.03	8.91	6.19	0.53	100.04	42.96	53.99	3.04
74b-22C[a]	55.96	28.17	0.11		0.53	0.07	10.69	5.26	0.27	101.21	52.05	46.37	1.58
74b-13R	58.35	25.87	0.04		0.51	0.04	8.72	6.23	0.55	100.39	42.24	54.58	3.17
2-2C	56.15	27.19	0.11		0.56	0.04	10.02	5.64	0.44	100.24	48.31	49.18	2.51
32-8R	58.12	26.23	0.27		0.60	0.04	8.23	6.57	0.63	100.80	39.42	56.99	3.59
74a-1C	57.38	26.52	0.11		0.64	0.05	9.28	6.08	0.52	100.72	44.42	52.63	2.95
74b-5R	59.33	25.56	0.07		0.53	0.07	7.84	6.66	0.60	100.75	38.03	58.52	3.45

[a]C, M, and R refer to core, mantle, and rim. Blank entries indicate below detection limit.

pigeonite prisms, up to 4 × 1 mm in size (Fig. 4a). The texture is more like that of a coarse-grained shergottite such as NWA 6963 (Filiberto et al. 2014) than that of most other shergottites, but NWA 6963 contains much more abundant augite than NWA 10414. The key question is why the augite found in other basaltic shergottites is present only as a minor interstitial phase. To investigate the origin of this cumulate, we compare its oxide and pyroxene compositions to those of other shergottites, and its earliest pyroxenes to pigeonite crystallized in calculations or experiments with potential parent liquids.

The chromite-ulvöspinel of olivine-phyric shergottites shown in Fig. 7 have a wide range of composition, from Cr-rich (associated with early olivine) to Cr-poor close to or on the Usp-Mag join (in their groundmass or mesostasis). Basaltic shergottites contain Ti-magnetite rather than chromite, except those with liquidus magnesian pyroxene like NWA 480 (Barrat et al. 2002a). NWA 10414 chromite-ulvöspinel is intermediate within this range with few analyses plotting near the Chr apex, and few near the Ti-Fe join (Fig. 7). The rock is thus intermediate between most olivine-phyric and basaltic shergottites. In addition, its Usp/Mag ratio resembles that of enriched and intermediate shergottites rather than that of the depleted shergottites Tissint and NWA 5789 (Fig. 7).

Pyroxene fractionation patterns reveal many differences between shergottites, as shown in the assembled pyroxene quadrilaterals of Mikouchi et al. (1999, fig. 3), Papike et al. (2009, fig. 10), and Meyer (2012).There are two styles of pyroxene crystallization in the basaltic shergottites (Mikouchi et al. 1999), (1) simple Fe enrichment in coexisting grains of pigeonite and augite and (2) sequential growth of magnesian pigeonite (or orthopyroxene) followed by augite mantles and ferroan

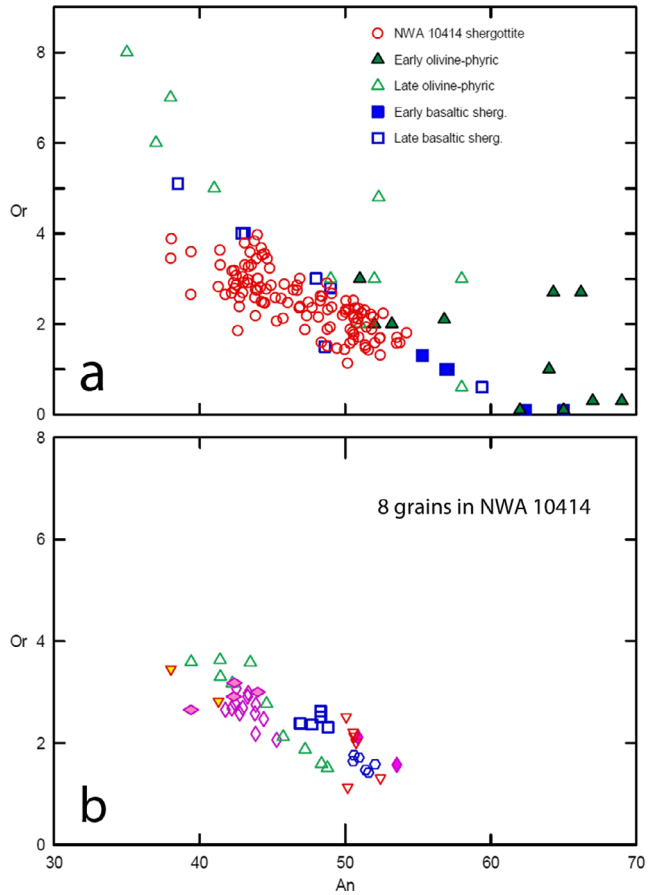

Fig. 6. Plagioclase (maskelynite) compositions in mol % An versus Or. a) Total range for Northwest Africa (NWA) 10414 compared to early- and late-crystallized plagioclase (cores and rims, or extremes of range) in other shergottites (see text for details). b) Eight individual grains in NWA 10414 differ in composition.

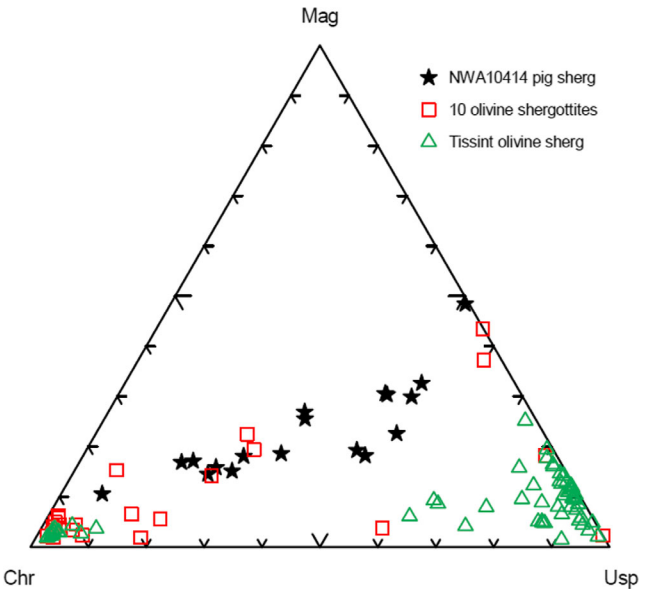

Fig. 7. The Cr-Ti spinel in Northwest Africa 10414 does not have the most Cr-rich compositions found in olivine-phyric shergottites, and it extends to the late Ti-magnetite typical of basaltic shergottites. See text for sources of shergottite data.

pigeonite rims on composite crystals. These trends are shown schematically in pyroxene quadrilaterals (Figs. 8a and 8b) based on data for Shergotty (Hale et al. 1999) and LAR 06319 (Basu Sarbadhikari et al. 2009; Peslier et al. 2010). Many of the basaltic shergottites like the classic Shergotty follow the first pattern (Papike et al. 2009; Meyer 2012). Others show a Ca enrichment in pigeonite followed by augite mantling (McSween et al. 1996; Mikouchi et al. 1998; Barrat et al. 2002a; Mikouchi and Barrat 2009); they have a complex pyroxene zoning trajectory, which is like that in olivine-phyric shergottites (Papike et al. 2009; Meyer 2012), and some Apollo 12 mare basalts (Kushiro et al. 1971), Apollo 15 quartz-normative basalts (Grove and Bence 1977), and terrestrial komatiites (Arndt and Fleet 1979). These differences in crystallization patterns were attributed by Mikouchi et al. (1999) to (1) near-equilibrium crystallization with no significant undercooling, and (2) rapid disequilibrium crystallization of undercooled magmas to give the complex zoning. A similar interpretation was used for the terrestrial and lunar occurrences.

The pyroxene in NWA 10414 is also broadly intermediate in composition between that of olivine-phyric and olivine-free shergottites, with the liquidus pigeonite Mg# higher than that in some basaltic shergottites and lower than that in many olivine-phyric shergottites. It shows modest enrichment toward the rims, in both Ca and Fe as in many olivine-phyric shergottites (Papike et al. 2009). However, the liquidus pigeonite composition in NWA 10414 ($En_{68}Fs_{27}Wo_5$) is not unique; the earliest crystallized pigeonites in some shergottites, both basaltic and olivine-phyric, are very similar (Fig. 8c). The most magnesian pyroxenes for Shergotty ($En_{68}Fs_{24}Wo_8$, Hale et al. 1999, fig. 3), EETA 79001B ($En_{70}Fs_{21}Wo_9$, Van Niekerk et al. 2007, fig. 6), NWA 1068 ($En_{72}Fs_{23}Wo_5$, Barrat et al. 2002b), NWA 6234 ($En_{70}Fs_{26}Wo_4$, Gross et al. 2013, NWA 6234), and LAR 06319 ($En_{71}Fs_{25}Wo_4$, Basu Sarbadhikari et al. 2009; Peslier et al. 2010) are all plotted as diamonds close to the most Mg-rich pigeonite in NWA 10414 (Fig. 8c). The above earliest pigeonites tend to be too poor in Ca and too magnesian to be in equilibrium with augite at liquidus temperatures for shergottite (Huebner 1980; Lindsley 1983). NWA 10414 pigeonite shows modest enrichment in both Fe and Ca, with rim pigeonite only slightly

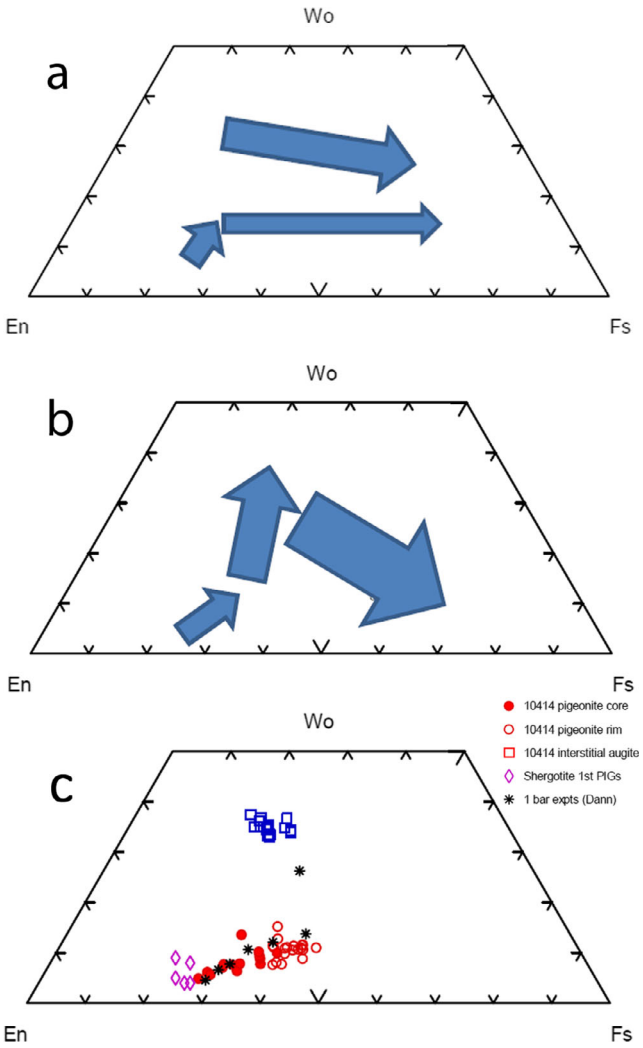

Fig. 8. Shergottite pyroxenes and Northwest Africa (NWA) 10414 pigeonite (a) co-crystallization of pigeonite and augite; schematic, after Hale et al. (1999). b) Complex zoning sequence in LAR06319; schematic, after Basu Sarbadhikari et al. (2009) and Peslier et al. (2010). c) Comparison of NWA 10414 pigeonite with the earliest (most magnesian) pigeonite in Shergotty, NWA 1068, NWA 6234, Elephant Moraine 79001B, and LAR 06319, all plotted as diamonds. See text for sources of data.

enriched in Ca in equilibrium with interstitial augite. Pigeonites in many other shergottites are either strongly enriched in Ca to augite mantles or in Fe to ferropigeonite. Among the shergottites with similar early pigeonite compositions, NWA 10414 most resembles the contact facies between EETA 79001 A and B in phase abundances: this zone has more pigeonite phenocrysts than the more evolved pyroxene assemblage in the main part of lithologic unit B (Goodrich 2003; Van Niekerk et al. 2007).

Crystallization Experiments and Modeling

Reproducing the crystallization of shergottites by experiment or modeling depends on knowing the parent liquid composition, which is difficult because most meteorites consist of liquid plus accumulated crystals. We consider possible liquid compositions for basaltic shergottites with similarities to NWA 10414. Crystallization experiments were performed by McKay et al. (2000) and by Dann et al. (2001) on SILC (Shergotty intercumulus liquid composition) calculated by subtracting pyroxene core composition from bulk composition for Shergotty (Hale et al. 1999). The experiments used a combined range of 1 bar to 2 kb with an oxygen fugacity relative to the fayalite-magnetite-quartz buffer (FMQ) of −1 to + 1 log units. Dann et al. (2001) estimated the crystallization pressure as 0.56 kb, as discussed below. For comparison purposes, we refer to experiments at 1 bar and FMQ, used in both studies. Pigeonite crystallizes from 1200 to 1110 °C (McKay et al. 2000, fig. 2) and 1175–1075 °C (Dann et al. 2001), where it is joined by augite. The composition of its liquidus pyroxene is $En_{67}Fs_{28}Wo_5$ (Dann et al. 2001) or $En_{66}Fs_{30}Wo_4$ (McKay et al. 2000), and it is very close to that of the most magnesian pigeonite compositions in NWA 10414 with a similar composition range (Fig. 8c).

Stolper and McSween (1979) and McCoy and Lofgren (1999) also showed experimentally that pigeonite crystallized before augite in melts with the compositions of bulk Shergotty and Zagami. Although pigeonite and augite are widely perceived as joint liquidus phases in such "basaltic" shergottites, they could have equilibrated mutually after the precipitation of augite joined pigeonite and after accumulation in the residual magma (Stolper and McSween 1979). The survival of magnesian pigeonite too poor in Ca to be in equilibrium with the augite in Shergotty (Hale et al. 1999) is consistent with this idea. McKay et al. (2000) considered their failure to produce the expected simultaneous crystallization of pigeonite and augite to be a paradox. However, as noted above, in some basaltic shergottites, pigeonite does crystallize before augite, particularly in those with the disequilibrium trend but even in Shergotty (Hale et al. 1999, fig. 4). Thus, we judge the experiments not to be paradoxical in the context of shergottites and other shergottite crystallization experiments, but their starting compositions need minor modification for Shergotty (more CaO, Dann et al. 2001) to accelerate the appearance of augite after pigeonite crystallization.

We modeled the crystallization of a number of shergottites at pressures between 1 bar and 2 kb, and oxygen fugacities between FMQ and FMQ-2 using

PETROLOG (Danyushevsky and Plechov 2011). This program calculates pseudo-liquidus temperatures using mineral-melt equilibria models for all possible minerals. We used the optional models of Sack et al. (1980) for melt oxidation state and Ariskin et al. (1993) for silicate mineral-melt equilibria. Calculated pseudo-liquidus temperatures are compared to determine which phase(s) should crystallize. Where PETROLOG indicated that orthopyroxene and pigeonite come onto the liquidus at the same temperature within error, we chose to crystallize pigeonite rather than orthopyroxene. We searched for liquids with pigeonite crystallizing alone, capable of forming cumulates, after the crystallization of any olivine and before the appearance of augite (or plagioclase). Although pressure changed crystallization temperature and Al content of pyroxene, it had a trivial effect on the calculated major element composition of pyroxene, so here we report only 1 bar calculations. The effect of a change of 2 log units in oxygen fugacity was ~1–4 mol% in Fs, with more ferroan pyroxene at the lower fO_2. We report below results for FMQ-2, except where otherwise stated, because they come closer to the composition of the pigeonite in NWA 10414 for the liquid compositions available.

We used PETROLOG first with basaltic shergottite compositions, starting with Zagami, and later with olivine-phyric shergottite potential parent melts, to search for extensive crystallization of pigeonite alone. The results are summarized in Figs. 9 and 10. We evaluated the use of PETROLOG for shergottites by comparing results for the crystallization of Zagami to those from experiments at 1 bar and FMQ (McCoy and Lofgren 1999). The liquidus temperatures are 1251 °C (PETROLOG) and 1255–1260 °C (McCoy and Lofgren); the first pigeonite compositions are FeO 14.1 versus 13.6 wt%, MgO 26.2 versus 26.8 wt%, and CaO 3.7 versus 2.5 wt%, respectively; the first augite appeared at 1169 °C versus 1175 °C, respectively. Although this confirms the utility of PETROLOG, both these pigeonite compositions are more magnesian than natural pigeonite compositions for Zagami (McCoy and Lofgren 1999) and NWA 10414 (Fig. 9a). The same is true for results shown in Figs. 9a and 9b for an oxygen fugacity of FMQ-2, probably because the bulk composition is not a true liquid composition (Stolper and McSween 1979).

Elephant Moraine A 79001B is a logical candidate for the parent liquid of NWA 10414, because of its pigeonite-rich border facies discussed above and their similar liquidus pigeonite compositions. Analyses of three relatively small samples (McSween and Jarosewich 1983; Warren et al. 1999; Arauza et al. 2010) gave slightly different compositions. We found using PETROLOG that they have different crystallization sequences, pigeonite then augite, plagioclase then augite, and pigeonite then plagioclase, respectively. These differences are easily understood because the EETA 79001B bulk composition(s) plot very close to the pigeonite-augite-plagioclase invariant point (Stolper and McSween 1979; Arauza et al. 2010; Jones and Arauza 2010). Furthermore, Van Niekerk et al. (2007) observed different crystallization sequences as a function of the distance from the contact with lithology A, underlining the difficulty of defining the parent liquid composition. Two of these composition estimates (McSween and Jarosewich 1983; Warren et al. 1999) are capable of producing a pigeonite cumulate, though only over a temperature range of ~30 °C. The McSween and Jarosewich composition is shown in Fig. 9a, because its cumulate would have interstitial plagioclase formed after than augite, as in NWA 10414. However, the solitary pigeonite calculated for this composition crystallized over a temperature range of only 32 °C (Fig. 9a) and is too restricted in Fe/Mg and too calcic compared to that in NWA 10414 (Fig. 10a).

We modeled the crystallization of the Shergotty parent SILC using PETROLOG and compared the results to those of MELTS calculations (Hale et al. 1999, fig. 5a). For 1 bar and FMQ, we have pigeonite on the liquidus at ~1201 °C (MELTS) and 1206 °C (PETROLOG), while pigeonite formed between 1190 and 1075 °C in the experiments of Dann et al. (2001). Augite appears at about 1121 °C (MELTS) as opposed to 1143 °C (PETROLOG), too early to match the augite-free composition range of pigeonite in NWA 10414. Crystallization with FMQ-2 matches much better, with all except the most magnesian compositions reproduced (Fig. 10a).

Second, we considered the parent melts of olivine-phyric shergottites. Fractional crystallization of EETA79001A groundmass composition E_g (McSween and Jarosewich 1983; Longhi and Pan 1989) yielded 15% olivine followed by 11% pigeonite, before the onset of augite at 1163 °C. The hypothetical pigeonite cumulate that could be formed has a composition that is too calcic and too restricted in Fe/Mg ratio to be a good match to NWA 10414 (Fig. 10b).

Northwest Africa 6234 is an olivine-phyric shergottite containing olivine microphenocrysts, pigeonite in the groundmass, and late interstitial augite, interpreted as a ferroan primary magma crystallized at upper crustal pressures (Gross et al. 2013). Modeling its crystallization using PETROLOG with FMQ + 2, a value between the extremes calculated for different mineral assemblages by Gross et al. (2013), yields a good match to the observed olivine and Ca-poor pyroxene compositions (Fig. S3 in supporting information). Applying the results to the crystallization

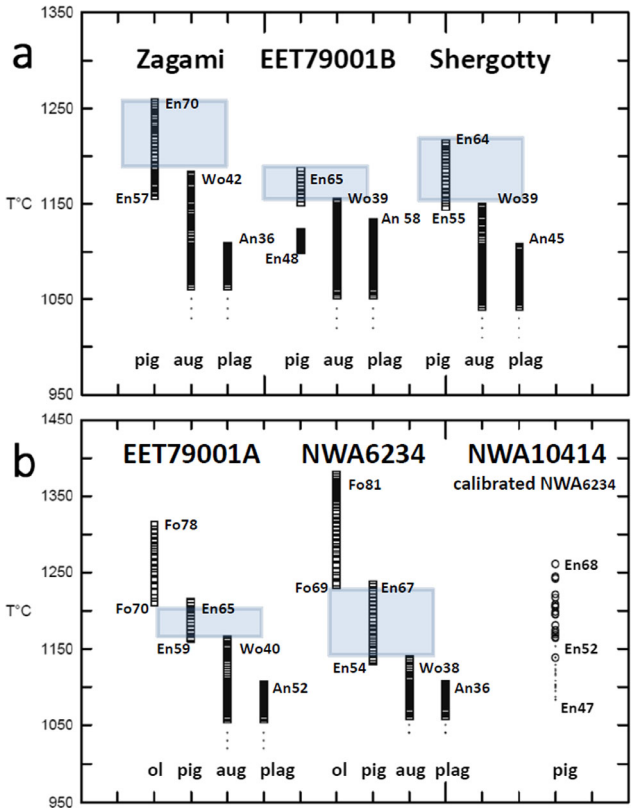

Fig. 9. Bar chart giving temperature ranges for the crystallization of olivine, pigeonite, augite, and plagioclase calculated using PETROLOG for 1 bar and fayalite-magnetite-quartz buffer-2 (a) olivine-free shergottites and (b) olivine-phyric shergottites. The estimated temperature range for Northwest Africa (NWA) 10414 pigeonite cores (open circles) and rims (dots) based on the calculated temperature–composition correlation for NWA 6234 pyroxene is also shown in (b). The rectangles indicate temperature windows with neither olivine nor augite, where formation of a pigeonite cumulate is possible. Details of starting compositions given in text.

of NWA10414, we find that the calculated pyroxene range also matches its pigeonite core compositions very well (Fig. 10b), better than with SILC.

Based on the similarity of the pigeonite compositions, we can estimate the temperature range of pigeonite in NWA 10414 using the regression line for En versus T °C from calculations on NWA 6234. This range (1261−1084 °C) is plotted in Fig. 10b for comparison with the temperature windows for solitary pigeonite crystallization calculated with PETROLOG for the other shergottites. We see that rim pigeonite (dots) continued to crystallize at similar temperatures to augite in many shergottites. The only obvious difference between calculated compositions for the first liquids saturated in pigeonite is that those in SILC and NWA 6234 had <10% CaO and those not reproducing our pyroxene composition range had >10% CaO, which tended to produce more calcic and more magnesian pigeonite before the appearance of augite.

Dann et al. (2001) constructed a phase diagram for SILC as a function of P_{H2O} (water pressure) and temperature (their fig. 1). This shows that in order to have pigeonite crystallize before augite, a low water pressure is required. Pigeonite crystallizes alone for ~60–95 °C at 0–0.5 kb, from this Shergotty parent liquid. Dann et al. (2001) used their high pressure phase compositions to estimate a crystallization pressure of Shergotty's two-pyroxene assemblage as 0.56 kb. As NWA 10414 has much the same range of pigeonite compositions as in the 1 bar experiments of Dann et al. (2001) over an estimated temperature range of 170 °C, with no augite present, it probably crystallized at near-surface conditions.

The pyroxene minor element data for equilibrium crystallization experiments on the SILC composition (Dann et al. 2001) also show that formation at water pressures of 1 bar and 2 kb cannot be distinguished using Al and Ti concentrations in pigeonite (Fig. S4 in supporting information). Ti/Al ratios in pyroxenes are affected by growth rate and co-crystallizing phases. A lunar quartz-normative basalt composition crystallized in the laboratory yielded pigeonite with a very similar composition range to that for NWA 10414 (Grove and Bence 1977). The Ti/Al ratios for their pigeonite crystallized at cooling rates between 1.75 and 60 °C/h deviate from the equilibrium value, increasing toward unity as the quench temperature is decreased, because plagioclase forms, incorporating Al. Pigeonite cores for NWA 10414 pigeonite have Ti/Al ratios similar to those for equilibrium crystallization of the lunar basalt. However, pigeonite rims have much higher ratios up to 0.8 (Fig. S2), also probably due to fractionation during rapid crystallization, consistent with the localized incorporation of small plagioclase crystals in the rims in a weak subophitic texture.

Formation of Pigeonite Cumulate Shergottite

Pigeonite is a Ca-poor pyroxene that has undergone the displacive transformation to the $P2_1/c$ space group and that on Earth occurs mainly in volcanic rocks, especially andesites (e.g., Deer et al. 1977) though also in komatiites (Arndt and Fleet 1979). On the Moon, it is found in mare basalts (Kushiro et al. 1971; Grove and Bence 1977). In plutonic and most hypabyssal rocks, pigeonite exsolves augite and inverts to orthopyroxene because of slow cooling (Hess 1960; Robinson 1980). The Palisades Sill of New Jersey, emplaced at a depth of ~3 km, shows inverted pigeonite with spectacular exsolved augite (Walker 1969). The

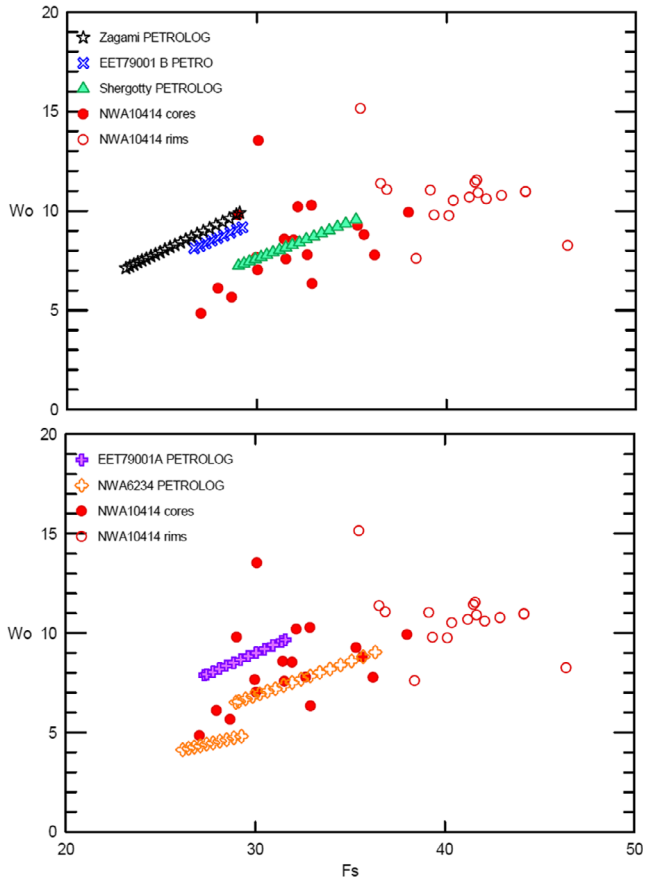

Fig. 10. Comparison of pigeonite composition for Northwest Africa (NWA) 10414 and pigeonite crystallized alone using PETROLOG at 1 bar and fayalite-magnetite-quartz buffer-2 for (a) basaltic shergottite parent liquids, and (b) olivine-phyric shergottite parent liquids. The best matches are obtained with (a) Shergotty intercumulus liquid composition (Hale et al. 1999) and (b) NWA 6234 (Gross et al. 2013).

widespread occurrence of primary pigeonite in shergottites is thus an indication that most of them are volcanic or subvolcanic rocks. NWA 10414 has a classic orthocumulate texture, but it differs from terrestrial pyroxene cumulates, and many diabases, in that pigeonite is present rather than inverted pigeonite, suggesting near-surface cooling.

There are basaltic shergottites with complex pyroxenes representing the rapid crystallization of liquid, shergottites with coexisting pyroxene pairs where crystal cores indicate a limited amount of accumulation, and NWA 10414 where the abundance of only the higher temperature pyroxene indicates a true cumulate. Shergottites with co-crystallized pigeonite and augite (Shergotty and Zagami) contain exsolution lamellae a few tens of nm wide in both pigeonite and augite, but those with disequilibrium pyroxene crystallization (EETA79001 and QUE94201) do not: their cooling must have been relatively rapid and extremely rapid, respectively, even in the subsolidus (Mikouchi et al. 1999). Brearley (1991) calculated that pyroxene exsolution in Zagami occurred during cooling at a rate of <0.02 °C/h and at a depth of >10 m. In NWA 10414, the augite lamellae in pigeonite are only ~100 nm wide, suggesting moderately rapid cooling in the subsolidus and a depth of some tens of meters.

Olivine-phyric EETA 79001 A may have been parental to the pigeonite-rich EETA 79001 B basaltic shergottite (Goodrich 2003). The crystallization of pigeonite earlier than augite in many shergottites, as documented above, provides the possibility of making a pigeonite cumulate after olivine has settled. This is the explanation specifically used by Van Niekerk et al. (2007) for the ~1 cm wide pigeonite-phyric contact facies of EET-B with EET-A. We illustrate the formation of a pigeonite cumulate in the context of the model of Van Niekerk et al. (2007) who envisaged eruption of an olivine-charged liquid in which olivine settled out before the solidification of an upper basaltic shergottite layer in the same flow (Fig. 11). We propose that NWA 10414 formed from a liquid like NWA6234 (Gross et al. 2013) but, for our purposes, it is not important if the olivine accumulated in a subvolcanic chamber, at the base of a thick single flow, or before the separation of a fractionated flow lobe. We illustrate the transport and accumulation of olivine in Figs. 11.1 and 2. The daughter liquid of NWA 6234 that precipitates pigeonite in Fig. 11.2 is quite similar to Shergotty SILC (Hale et al. 1999) after olivine fractionation, and both compositions are Ca-poor compared to other proposed parents. The pigeonite on the liquidus has a sufficient temperature interval to form a cumulate (Fig. 9), as shown in Fig. 11.3. The contact above the olivine cumulate in Fig. 11.3 would be like that in EET-A/B if crystallization occurred in a static flow or very shallow magma chamber, but with greater depth and slower cooling, more extensive pigeonite settling would have occurred. Augite and plagioclase crystallize along with pigeonite in the liquid overlying the pigeonite cumulate liquid (Fig. 11.4). If drained away, this liquid could have produced a normal basaltic shergottite flow and allowed the underlying cumulate to cool relatively rapidly (Richter et al. 2016). In summary, the fractionation of NWA 6234 liquid could have produced an olivine accumulation, not unlike EET-A, then a pigeonite cumulate (like NWA 10414), and subsequent daughter liquid could have formed fractionated basaltic shergottites. NWA 10414 captures the temperature interval in the solidification of a shergottite magma when olivine has ceased, but augite and plagioclase have not begun to crystallize.

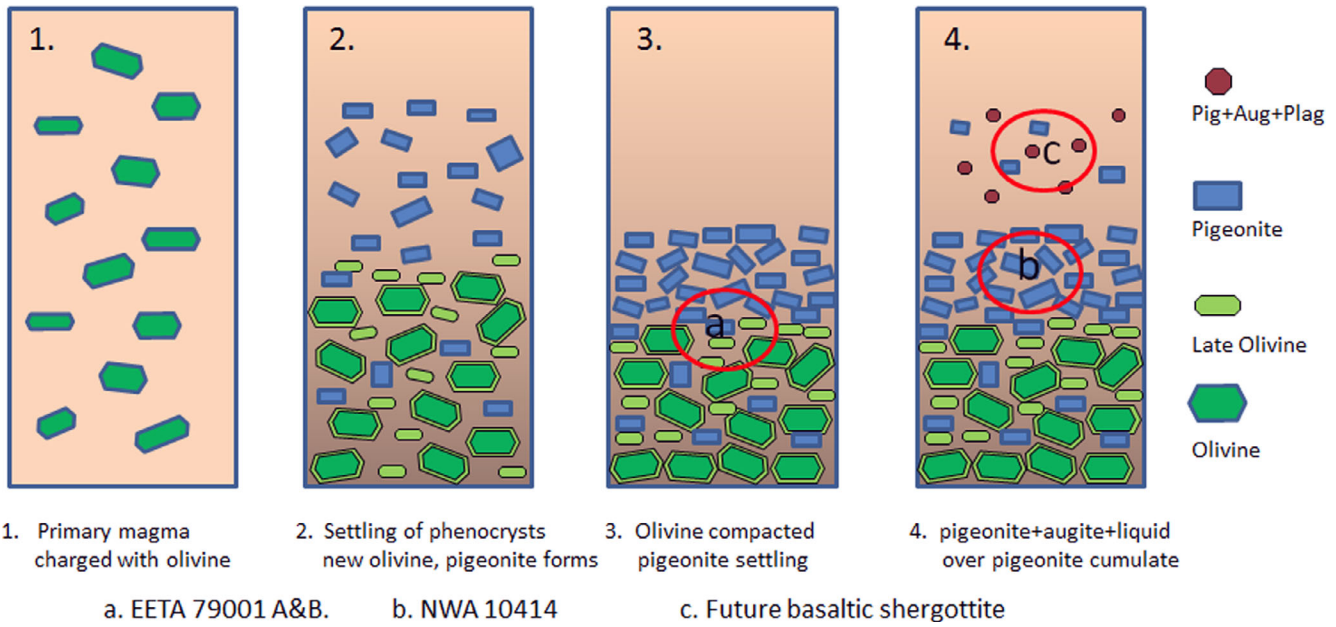

Fig. 11. Formation of Northwest Africa (NWA) 10414 pigeonite from olivine-phyric liquid NWA86234, simplified after the model of Van Niekerk et al. (2007) for Elephant Moraine (EET) 79001. 1. A magma charged with olivine phenocrysts reaches a near-surface environment. 2. Olivine settles; pigeonite crystallizes in the daughter liquid. 3. Pigeonite accumulates. Point "a" is analogous to EET-A and the pigeonite-rich border of EET-B. 4. Pigeonite cumulate "b" is analogous to NWA 10414. Pigeonite, augite, and plagioclase crystallize in the daughter liquid in "c" to form a later basaltic shergottite.

CONCLUSIONS

Northwest Africa 10414 is a so-far unique pigeonite cumulate shergottite, containing 73% pigeonite, no olivine, and only ~3% interstitial augite. However, there are similarities in mineral abundances to a 1 cm pigeonite-rich contact zone between EET 79001 olivine-phyric and basaltic facies, A and B (Van Niekerk et al. 2007), and in texture to NWA 6963 (Filiberto et al. 2014).

Its chromite-ulvöspinel compositions extend from near the most Cr-rich compositions found in olivine shergottites to the Ti-magnetite of basaltic shergottites. The composition of the most magnesian pigeonite cores is $En_{68}Fs_{27}Wo_5$, similar to the earliest pyroxenes for basaltic shergottites Shergotty ($En_{68}Fs_{24}Wo_8$, Hale et al. 1999, fig. 4) and EET 79001B ($En_{65}Fs_{27}Wo_8$, Mikouchi et al. 1998; Van Niekerk et al. 2007), and for olivine-phyric shergottites NWA 1068 ($En_{72}Fs_{23}Wo_5$, Barrat et al. 2002b), NWA 6234 (Gross et al. 2013, $En_{70}Fs_{26}Wo_4$), and LAR 06319 ($En_{71}Fs_{25}Wo_4$, Basu Sarbadhikari et al. 2009; Peslier et al. 2010). Its most calcic maskelynite composition is $An_{53.6}Ab_{44.7}Or_{1.7}$, more sodic than the most calcic plagioclase in most other shergottites.

The NWA 10414 most magnesian pigeonite composition is similar to that of the liquidus pigeonite ($En_{67}Fs_{28}Wo_5$) of a Shergotty parent liquid SILC at 1 bar and FMQ (Dann et al. 2001) that crystallizes pigeonite in cooling through 100 °C, before co-crystallizing with augite. The range of pigeonite compositions can be matched by crystallization with PETROLOG at 1 bar and FMQ-2, quite well for the SILC basaltic composition, and very well for the NWA 6234 olivine-phyric liquid composition, after the end of olivine crystallization.

The juxtaposition of pigeonite-phyric shergottite with olivine-phyric shergottite (Van Niekerk et al. 2007) and the phase relations for shergottites suggest the formation of NWA 10414 from an olivine-saturated parent liquid. After olivine crystallization from a liquid composition like NWA 6234, accumulation of pigeonite could have occurred from a resulting daughter liquid quite like SILC. NWA 10414 is a link between olivine-phyric and basaltic shergottites.

Acknowledgments—We are indebted to L. Labenne for the sample and his insights; to M. Fialin and N. Rividi for help with the electron probe analyses; to N. Castle and two anonymous reviewers for thorough, critical, and very helpful reviews which led to much improvement of the manuscript; to M. J. Carr for IGPET, as always; and to L. Danyushevsy for PETROLOG. We are grateful for funding through ANR grant MARS-PRIME ANR-16-CE31-0012 (P.I. N. Mangold).

Editorial Handling—Dr. Cyrena Goodrich

REFERENCES

Arauza S. J., Jones J. H., Mittlefehldt D. W., and Le L. 2010. Is EETA79001 Lithology B a true melt composition? (abstract #1429) 41st Lunar and Planetary Science Conference. CD-ROM.

Ariskin A. A., Frenkel M. Y., Barmina G. S., and Nielsen R. 1993. COMAGMAT: A Fortran program to model magma differentiation processes. *Computers & Geosciences* 19:1155–1170.

Arndt N. T. and Fleet M. E. 1979. Stable and metastable pyroxene crystallization in layered komatiite lava flows. *American Mineralogist* 64:856–864.

Barrat J. A., Gillet P., Sautter V., Jambon A., Javoy M., Göpel C., Lesourd M., Keller F., and Petit E. 2002a. Petrology and chemistry of the basaltic shergottite Northwest Africa 480. *Meteoritics & Planetary Science* 37:487–499.

Barrat J. A., Jambon A., Bohn M., Gillet P., Sautter V., Göpel C., Lesourd M., and Keller F. 2002b. Petrology and chemistry of the picritic shergottite Northwest Africa 1068. *Geochimica et Cosmochimica Acta* 66:3505–3518.

Basu Sarbadhikari A., Day J. M. D., Liu Y., Rumble D. III, and Taylor L. A. 2009. Petrogenesis of olivine-phyric shergottite LAR 06319: Implications for enriched components in Martian basalts. *Geochimica et Cosmochimica Acta* 73:2190–2214.

Bogard D. D. and Johnson P. 1983. Martian gases in an Antarctic meteorite? *Science* 221:651–654.

Brearley A. J. 1991. Subsolidus microstructure and cooling history of pyroxenes in the Zagami shergottite (abstract). 22nd Lunar and Planetary Science Conference pp. 135–136.

Bridges J. C. and Warren P. H. 2006. The SNC meteorites: Basaltic igneous processes on Mars. *Journal of the Geological Society* 163:229–251.

Buddington A. F. and Lindsley D. H. 1964. Iron–titanium oxide minerals and synthetic equivalents. *Journal of Petrology* 5:310–357.

Bunch T. E., Irving A. J., Wittke J. H., Rumble D., Korotev R. L., Gellissen M., and Palme H. 2009. Petrology and composition of Northwest Africa 2990: A new type of fine-grained enriched, olivine-phyric shergottite (abstract #2274). 40th Lunar and Planetary Science Conference. CD-ROM.

Chennaoui Aoudjehane H., Avice G., Barrat J.-A., Boudouma O., Chen G., Duke M. J. M., Franchi I. A., Gat-tacecca J., Grady M. M., Greenwood R. C., Herd C. D. K., Hewins R. H., Jambon A., Marty B., Rochette P., Smith C. L., Sautter V., Verchovsky A., Weber P., and Zanda B. 2012. Tissint Martian meteorite: A fresh look at the interior, surface and atmosphere of Mars. *Science* 338:785–788.

Dann J. C., Holzheid A. H., Grove T. L., and McSween H. Y. 2001. Phase equilibria of the Shergotty meteorite: Constraints on pre-eruptive water contents of Martian magmas and fractional crystallization under hydrous conditions. *Meteoritics & Planetary Science* 36:793–806.

Danyushevsky L. V. and Plechov P. 2011. Petrolog 3: Integrated software for modeling crystallization processes. *Geochemistry, Geophysics, Geosystems* 12:Q07021.

Deer W. A., Howie R. A., and Zussman J. 1977. *Rock-forming minerals: Single-chain silicates*. vol. 2A. London, UK: Geological Society. p. 680.

de la Peña F., Ostasevicius T., Fauske V. T., Burdet P., Jokubauskas P., Nord M., Sarahan M., Prestat E., Johnstone D. N., Taillon J., and Caron J. 2017. Electron microscopy (big and small) data analysis with the open source software package HyperSpy. *Microscopy and Microanalysis* 23:214–215.

El Goresy A., Gillet P. H., Miyahara M., Ohtani E., Ozawa S., Beck P., and Montagnac G. 2013. Shock-induced deformation of Shergottites: Shock-pressures and perturbations of magmatic ages on Mars. *Geochimica et Cosmo-Chimica Acta* 101:233–262.

Filiberto J. and Dasgupta R. 2011. Fe^{2+}-Mg partitioning between olivine and basaltic melts: Applications to genesis of olivine-phyric shergottites and conditions of melting in the Martian interior. *Earth and Planetary Science Letters* 304:527–537.

Filiberto J., Chin E., Day J. M. D., Franchi I. A., Greenwood R. C., Gross J., Penniston-Dorland S. C., Schwenzer S. P., and Treiman A. H. 2012. Geochemistry of intermediate olivine-phyric shergottite Northwest Africa 6234, with similarities to basaltic shergottite Northwest Africa 480 and olivine-phyric shergottite Northwest Africa 2990. *Meteoritics & Planetary Science* 47:1256–1273.

Filiberto J., Gross J., Trela J., and Ferré E. C. 2014. Gabbroic shergottite Northwest Africa 6963: An intrusive sample of Mars. *American Mineralogist* 99:601–606.

Filiberto J., Gross J., Udry A., Trela J., Wittmann A., Cannon K. M., Penniston-Dorland S., Ash R., Hamilton V. E., Meado A. L., Carpenter P., Jolliff B., and Ferré E. C. 2018. Shergottite Northwest Africa 6963: A pyroxene-cumulate Martian gabbro. *Journal of Geophysical Research: Planets* 123:1823–1841.

Fritz J., Greshake A., and Stöffler D. 2005. Micro-Raman spectroscopy of plagioclase and maskelynite in Martian meteorites: Evidence of progressive shock metamorphism. *Antarctic Meteorite Research* 18:96–116.

Goodrich C. A. 2002. Olivine-phyric Martian basalts: A new type of shergottite. *Meteoritics & Planetary Science* 37: B31–B34.

Goodrich C. A. 2003. Petrogenesis of olivine-phyric shergottites Sayh al Uhaymir 005 and Elephant Moraine A79001 lithology A. *Geochimica et Cosmochimica Acta* 67:3737–3771.

Goodrich C. A., Herd C. D., and Taylor L. A. 2003. Spinels and oxygen fugacity in olivine-phyric and lherzolitic shergottites. *Meteoritics & Planetary Science* 38:1773–1792.

Greshake A., Fritz J., and Stöffler D. 2004. Petrology and shock metamorphism of the olivine-phyric shergottite Yamato 980459: Evidence for a two-stage cooling and a single-stage ejection history. *Geochimica et Cosmochimica Acta* 68:2359–2377.

Gross J., Treiman A. H., Filiberto J., and Herd C. D. 2011. Primitive olivine-phyric shergottite NWA 5789: Petrography, mineral chemistry, and cooling history imply a magma similar to Yamato 980459. *Meteoritics & Planetary Science* 46:116–133.

Gross J., Filiberto J., Herd C. D., Daswani M. M., Schwenzer S. P., and Treiman A. H. 2013. Petrography, mineral chemistry, and crystallization history of olivine-phyric shergottite NWA 6234: A new melt composition. *Meteoritics & Planetary Science* 48:854–871.

Grove T. L. and Bence A. E. 1977. Experimental study of pyroxene-liquid interaction in quartz-normative bas-alt

15597. Proceedings, 8th Lunar and Planetary Science Conference. pp. 1549–1579.
Hale V. P. S., McSween H. Y., and McKay G. A. 1999. Re-evaluation of intercumulus liquid composition and oxidation state for the Shergotty meteorite. *Geochimica et Cosmochimica Acta* 63:1459–1470.
Herd C. D. 2003. The oxygen fugacity of olivine-phyric Martian basalts and the components within the mantle and crust of Mars. *Meteoritics & Planetary Science* 38:1793–1805.
Herd C. D. K., Papike J. J., and Brearley A. J. 2001. Oxygen fugacity of Martian basalts from electron microprobe oxygen and TEM-EELS analyses of Fe-Ti oxides. *American Mineralogist* 86:1015–1024.
Herd C. D. K., Walton E. L., Agee C. B., Muttik N., Ziegler K., Shearer C. K., Bell A. S., Santos A. R., Burger P. V., Simon J. I., Tappa M. J., McCubbin F. M., Gattacceca J., Lagroix F., Sanborn M. E., Yin Q.-Z., Cassata W. S., Borg L. E., Lindvall R. E., Kruijer T. S., Brennecka G. A., Kleine T., Nishiizumi K., and Caffee M. W. 2017. The Northwest Africa 8159 Martian meteorite: Expanding the Martian sample suite to the early Amazonian. *Geochimica et Cosmochimica Acta* 218:1–26.
Hess H. H. 1960. Stillwater Igneous Complex, Montana, a quantitative mineralogical study. Geological Society of America. *Memoir* 80:230.
Huebner S. S. 1980. Pyroxene Phase equilibria at low pressure. *Reviews in Mineralogy* 7:213–288.
Hui H., Peslier A. H., Lapen T., Shafer J. T., Brandon A. D., and Irving A. J. 2011. Petrogenesis of basaltic shergottite Northwest Africa 5298: Closed-system crystallization of an oxidized mafic melt. *Meteoritics & Planetary Science* 46:1313–1328.
Jones J. H. and Arauza S. J. 2010. The parent liquid of EET 79001, Lithology B (abstract #5331). *Meteoritics & Planetary Science* 45:A96.
Kushiro I. K., Nakamura Y. A., Kitayama K. E., and Akimoto S. I. 1971. Petrology of some Apollo 12 crystalline rocks. Proceedings of 2nd Lunar Science Conference. pp. 481–495.
Lanari P., Vidal O., De Andrade V., Dubacq B., Lewin E., Grosch E., and Schwartz S. 2014. XMapTools: A MATLAB©-based program for electron microprobe X-ray image processing and geothermobarometry. *Computers and Geosciences* 62:227–240.
Lapen T. J., Righter M., Andreasen R., Irving A. J., Satkoski A. M., Beard B. L., Nishiizumi K., Jull A. J. T., and Caffee M. W. 2017. Two billion years of magmatism recorded from a single Mars meteorite ejection site. *Science Advances* 3:e1600922.
Lindsley D. H. 1983. Pyroxene thermometry. *American Mineralogist* 68:477–493.
Longhi J. and Pan V. 1989. The parent magmas of the SNC meteorites. Proceedings, 19th Lunar and Planetary Science Conference. pp. 451–464.
McCoy T. J. and Lofgren G. E. 1999. Crystallization of the Zagami shergottite: An experimental study. *Earth and Planetary Science Letters* 173:397–411.
McKay G., Mikouchi T., Le L., Schwandt C., and Hashimoto M. 2000. The Shergotty paradox: An experimental perspective on intercumulus melt compositions (abstract #2000). 31st Lunar and Planetary Science Conference. CD-ROM.
McSween H. Y. Jr. and Jarosewich E. 1983. Petrogenesis of the Elephant Moraine A79001 meteorite: Multiple magma pulses on the shergottite parent body. *Geochimica et Cosmochimica Acta* 47:1501–1513.
McSween H. Y. Jr. Taylor L. A., and Stolper E. M. 1979a. Allan Hills 77005: A new meteorite type found in Antarctica. *Science* 204:1201–1203.
McSween H. Y. Jr, Stolper E. M., Taylor L. A., Muntean R. A., O'Kelley G. D., Eldridge J. S., Biswas S., Ngo H. T., and Lipschutz M. E. 1979b. Petrogenetic relationship between Allan Hills 77005 and other achondrites. *Earth and Planetary Science Letters* 45:275–284.
McSween H. Y. Jr, Eisenhour D. D., Taylor L. A., Wadhwa M., and Crozaz G. 1996. QUE94201 shergottite: Crystallization of a Martian basaltic magma. *Geochimica et Cosmochimica Acta* 60:4563–4569.
Meyer C. 2012. The Martian Meteorite Compendium. http://curator.jsc.nasa.gov/antmet/mmc/index.cfm. Accessed February 7, 2018.
Mikouchi T. and Barrat J. A. 2009. NWA 5029 basaltic shergottite: A clone of NWA 480/1460? *Meteoritics & Planetary Science Supplement* 72:5344.
Mikouchi T., Miyamoto M., and McKay G. A. 1998. Mineralogy of Antarctic basaltic shergottite QUE94201: Similarities to EETA79001 (Lithology B) Martian meteorite. *Meteoritics & Planetary Science* 33:181–189.
Mikouchi T., Miyamoto M., and McKay G. A. 1999. The role of undercooling in producing igneous zoning trends in pyroxenes and maskelynites among basaltic Martian meteorites. *Earth and Planetary Science Letters* 173:235–256.
Mikouchi T., Miyamoto M., and McKay G. A. 2001. Mineralogy and petrology of the Dar al Gani 476 Martian meteorite: Implications for its cooling history and relationship to other shergottites. *Meteoritics & Planetary Science* 36:531–548.
Mikouchi T., Koizumi E., McKay G., Monkawa A., Ueda Y., Chokai J., and Miyamoto M. 2004. Yamato 980459: Mineralogy and petrology of a new shergottite-related rock from Antarctica. *Antarctic Meteorite Research* 17: 13–34.
Musselwhite D. S., Dalton H. A., Kiefer W. S., and Treiman A. H. 2006. Experimental petrology of the basaltic shergottite Yamato 980459: Implications for the thermal structure of the Martian mantle. *Meteoritics & Planetary Science* 41:1271–1290.
Papanastassiou D. A. and Wasserburg G. J. 1974. Evidence for late formation and young metamorphism in the achondrite Nakhla. *Geophysical Research Letters* 1:23–26.
Papike J. J., Karner J. M., and Shearer C. K. 2003. Determination of planetary basalt parentage: A simple technique using the electron microprobe (abstract #2018). 34th Lunar and Planetary Science Conference. CD-ROM.
Papike J. J., Karner J. M., Shearer C. K., and Burger P. V. 2009. Silicate mineralogy of Martian meteorites. *Geochimica et Cosmochimica Acta* 73:7443–7485.
Peslier A. H., Hnatyshin D., Herd C. D. K., Walton E. L., Brandon A. D., Lapen T. J., and Shafer J. T. 2010. Crystallization, melt inclusion, and redox history of a Martian meteorite: Olivine-phyric shergottite Larkman Nunatak 06319. *Geochimica et Cosmochimica Acta* 74:4543–4576.
Reid A. M. and Bunch T. E. 1975. The nakhlites, part II: Where, when, and how. *Meteoritics* 10:317–324.
Richter F., Chaussidon M., Mendybaev R., and Kite E. 2016. Reassessing the cooling rate and geologic setting of Martian meteorites MIL 03346 and NWA 817. *Geochimica et Cosmochimica Acta* 182:1–23.

Robinson P. 1980. The composition space of terrestrial pyroxenes; internal and external limits. *Reviews in Mineralogy and Geochemistry* 7:419–494.

Sack R. O., Carmichael I. S. E., Rivers M. L., and Ghiorso M. S. 1980. Ferric-ferrous equilibria in natural silicate liquids at 1 bar. *Contributions to Mineralogy and Petrology* 75:369–376.

Sauerzapf U., Lattard D., Burchard M., and Engelmann R. 2008. The titanomagnetite–ilmenite equilibrium: New experimental data and thermo-oxybarometric application to the crystallization of basic to intermediate rocks. *Journal of Petrology* 49:1161–1185.

Shearer C. K., Burger P. V., Papike J. J., Borg L. E., Irving A. J., and Herd C. 2008. Petrogenetic linkages among Martian basalts. Implications based on trace element chemistry of olivine. *Meteoritics & Planetary Science* 43:1241–1258.

Stolper E. M. and McSween H. Y. Jr 1979. Petrology and origin of the shergottite meteorites. *Geochimica et Cosmochimica Acta* 43:1475–1498.

Treiman A. H. and Filiberto J. 2015. Geochemical diversity of shergottite basalts: Mixing and fractionation, and their relation to Mars surface basalts. *Meteoritics & Planetary Science* 50:632–648.

Van Niekerk D., Goodrich C. A., Taylor G. J., and Keil K. 2007. Characterization of the lithological contact in the shergottite EETA79001—A record of igneous differentiation processes on Mars. *Meteoritics & Planetary Science* 42:1751–1762.

Wager L. R., Brown G. M., and Wadsworth W. J. 1960. Types of igneous cumulates. *Journal of Petrology* 1:73–85.

Walker K. R.. 1969. *The Palisades Sill, New Jersey: A reinvestigation*. GSA Special Paper 111. Washington D.C.: Geological Society of America. 178 pp.

Walton E. L., Irving A. J., Bunch T. E., Kuehner S. M., Korotev R. L., and Herd C. D. K. 2012. Northwest Africa 4797: A strongly shocked ultramafic poikilitic shergottite related to compositionally intermediate Martian meteorites. *Meteoritics & Planetary Science* 47:1449–1474.

Warren P. H., Kallemeyn G. W., and Kyte F. T. 1999. Origin of planetary cores: Evidence from highly sidero-phile elements in Martian meteorites. *Geochimica et Cosmochimica Acta* 63:2105–2122.

Warren P. H., Greenwood J. P., and Rubin A. E. 2004. Los Angeles: A tale of two stones. *Meteoritics & Planetary Science* 39:137–156.

Wittke J. H., Bunch T. E., Herd C. D. K., Lapen T. J., Rumble D., Irving A. J., and Pitt D. 2010. Petrology and composition of "enriched" mafic Shergottite Northwest Africa 5718: Contrasts with Northwest Africa 2975/2986 (abstract #5313). *Meteoritics & Planetary Science* 45: A217.

Zanetta P.-M., Le Guillou C., Leroux H., Zanda B., Hewins R. H., Lewin E., and Pont S. 2019. Modal abundance, density and chemistry of micrometer-sized assemblages by advanced electron microscopy: Application to chondrites. *Chemical Geology* 514:27–41.

SUPPORTING INFORMATION

Additional supporting information may be found in the online version of this article:

Fig. S1. Phase cartography of NWA 10414 based on Si, Fe, Mg, and Ca K_α X-ray maps.

Fig. S2. Phase cartography of NWA 10414 with binned 1.77 μm pixels, based on nine-element X-ray maps.

Fig. S3. Olivine and pyroxene compositions in NWA6234 (Gross et al. 2013) compared with those calculated for the crystallization of liquid of bulk composition, using PETROLOG at 1 bar and FMQ-2.

Fig. S4. Pigeonite crystallized from Shergotty SILC by Dann et al. (2001) shows no systematic variation of Al and Ti as a function of water pressure, and NWA 10414 pigeonite is similar in composition.

Table S1. Compositions of parent liquids used in crystallization calculations with PETROLOG.